KSCE Journal of Civil Engineering (2020) 24(10):3105-3118
DOI 10.1007/s12205-020-1448-5

pISSN 1226-7988, eISSN 1976-3808
www.springer.com/12205

Tunnel Engineering

Failure Mechanism of Face for Slurry Shield-Driven Tunnel in Sand

Handong Liu[a], **Yafeng Zhang**[a], **and Haining Liu**[a]

[a]*Henan Key Laboratory of Geotechnical and Structural Engineering, North China University of Water Resources and Electric Power, Zhengzhou 450046, China*

ARTICLE HISTORY

Received 23 August 2019
Revised 1st 15 February 2020
Revised 2nd 23 April 2020
Accepted 29 May 2020
Published Online 14 August 2020

KEYWORDS

Slurry shield tunneling
Excavation face stability
Model test
PFC^{2D}
Soil arching effect
Limit support pressure

ABSTRACT

To achieve the failure mechanism of face for slurry shield tunnel in sand stratum, a model test device for shield excavation with ideal slurry film was developed. The active failure processes of tunnel excavation face in dry sand stratum for different densities and cover depths were achieved through model test and two-dimensional particle flow code (PFC^{2D}). Furthermore, soil deformation, failure mode and soil arching effect of tunnel excavation face were revealed. The results show that the face deformation can be divided into three stages in relation to the support pressure and the excavation face has been failed in third stage. The density of sand has a great influence on the failure mode of excavation face. The failure mode in dense condition is a combination of a wedge with slip arc and a prism chimney, while in loose condition it is a relatively dispersed "trumpet" shape failure zone. However, the cover depth has a negligible effect on the failure mode. In dense sand stratum, a loose failure zone was formed in front of the excavation face and a soil arch was formed above it. The soil arch developed continuously above the tunnel crown to the ground surface. The limit support pressure calculated by PFC^{2D} (two-dimensional particle flow code) increases with the cover depth, which is consistent with the observations in model tests.

1. Introduction

In recent years, because of its better adaptability to complex strata and high ground water level compared with other tunnel construction methods, slurry shield tunneling have been widely used for urban subway tunnels, cross-river tunnels, and subsea tunnels, especially in sand or sand-pebble strata, e.g., the Shanghai Yangtze River Cross-river Tunnel (Wang, 2008) and the Nanjing Yangtze River Cross-river Tunnel (Min et al., 2015). In the process of slurry shield tunneling, slurry infiltrates into stratum, when an impervious or slightly permeable film was formed (Broere and van Tol, 2000). Slurry film can not only prevent the groundwater, but also transform slurry pressure into support pressure, so as to balance the earth and water pressure in front of the excavation face (Anagnostou and Kovári, 1994; Min et al., 2013). Too low slurry pressure would lead to the failure of excavation face, which would not only cause surface settlement and collapse, but affect the surrounding buildings, structures and pipeline rupture. Therefore, how to set the slurry pressure is one of the most important issues to ensure the face stability.

The main research methods to study the face stability include theoretical analysis, physical model test and numerical analysis. Some theoretical analysis models, i.e., limit equilibrium models and upper-bound solutions have been proposed. Horn (1961) proposed the silo-shaped failure mode composed of a wedge and a prism. According to the theory proposed by Horn, Anagnostou and Kovári (1994, 1996) put forward the wedge failure mode for slurry shield tunnel and earth pressure balance (EPB) shield tunnel. Leca and Dormieux (1990) proposed dynamic field of face failure, obtained the polylines failure mode. Soubra (2000) proposed three-dimensional failure mode of multi cone on the basis of Leca's three-dimensional dynamic field. Subrin and Wong (2002) put forward the three-dimensional collapse mode in the shape of "Horn Tip".

Centrifuge and constant gravity model tests were also conducted to study the tunnel face stability. Chambon and Corté (1994) used seal membrane to simulate the support of excavation face and the instability of the tunnel face in sand was studied by centrifugal model test. Lee et al. (2006) studied the cross section shape of failure area in sand. Kirsch (2010) applied the digital

CORRESPONDENCE Yafeng Zhang 996727412@qq.com Henan Key Laboratory of Geotechnical and Structural Engineering, North China University of Water Resources and Electric Power, Zhengzhou 450046, China

image correlation (DIC) technique to the stability model test of excavation face, achieved the failure mode and minimum support pressures in dry sand with different density. Ahmed and Iskander (2012) obtained that the failure of shield excavation face was divided into several steps: deformation of excavation face, local sliding of excavation face and overall collapse of excavation face. Idinger et al. (2011) obtained the conclusion that there is soil arching effect for shallow tunnel. Chen et al. (2013) conducted several model tests under different buried depth ratio in dry sand stratum, analyzed the influence of C/D on limit support pressure on excavation face and ground settlement. Lv et al. (2018) conducted three groups of tests under different buried depths, including dry sand test under undrained condition, saturated sand test under undrained condition and considering seepage condition, obtained the failure mode and seepage characteristics under three working conditions.

The numerical method applied to study excavation face stability was mostly finite element method (FEM). Vermeer et al. (2002) studied the influence of uniform support pressure on the deformation and failure of excavation surface by dimensionless coefficient support stress ratio. Li et al. (2009) used FLAC^{3D} to study the active and passive failure modes of slurry shield excavation face, and considered the influence of slurry volume weight. Lv et al. (2017) studied the face stability for the shallow excavation tunnel by the coupling numerical simulation method of deformation and seepage, modified the wedge model and calculated the limit support pressure. Some investigators have applied discrete element method (DEM) to the excavation face failure for shield tunnel as it can reveal the failure microscopic mechanism of medium. Chen et al. (2011) studied the stability of shallow tunnel excavation face in dry sand stratum by DEM, discussed the relationship between limit support pressure and failure zone distribution as well as the burial depth. Zhang et al. (2011) studied the failure mechanism for slurry shield under different strata by PFC^{2D}. Wu et al. (2013) explored the design theory of cutter head excavation system of EPB by PFC^{3D}.

Stability of tunnel excavation face is greatly affected by the soil arch above it (Lee et al., 2006; Chen et al., 2011). The most well-known theory of earth arch was put forward by Terzaghi (1936). Dancygier et al. (2016) put forward a model to analyze the response of tunnel lining vault under the action of surface static load. Zhang et al. (2016) put forward a new earth pressure calculation model, which is improved on the basis of the original Terzaghi arch model. Ji et al. (2018) refined the silo based model, proposed an improved arch model to estimate the vertical pressure of the loose soil in the upper part of the pipeline under the condition of deep burial.

Up to now, the studies on face stability of slurry shield were mainly focused on limit slurry pressure and ground settlement regularity, while the model tests related to the failure mode and failure process were rarely reported. In addition, most of the previous studies used the FEM to study the face stability, rarely involving the microscopic failure mechanism for excavation face. Consequently, further research on excavation face stability of slurry shield conducted by model test and DEM is required for theoretical research and engineering practice. In this paper, physical model test and PFC simulation were conducted for various densities and burial depth ratios C/D=0.5, 1.0, and 2.0 (C is the cover depth and D is the diameter of tunnel) to achieve the failure mechanism of face for slurry shield-driven tunnel in sand. In the model test, the impermeable latex membrane was used to simulate the ideal slurry film and the active instability process of excavation face was realized by stress control method. The active failure processes of tunnel excavation face were achieved through model test and PFC^{2D}. Furthermore, soil deformation, failure mode and soil arching effect of tunnel excavation face were revealed.

2. Physical Model Tests

2.1 Model Device

In the laboratory experiments of tunnel excavation face stability, there are two major approaches to realize the failure of tunnel excavation face, i.e., stress and displacement control method. The stress control method was mainly rigid lining combined with flexible excavation face. Active or passive failure of excavation face can be realized through changing support pressure simulated by air or water pressure (Chambon and Corté, 1994; Yoo and Shin, 2002; Lee et al., 2006; Ahmed and Iskander, 2012). In the displacement control method, the excavation face was mostly rigid, which can realize the excavation face failure by piston movement (Kirsch, 2010; Idinger et al., 2011; Chen et al., 2013; Liu et al., 2017; Lv et al., 2018). Although the failure shape of excavation face can be achieved by displacement control method, the active failure process could not be realized. The excavation face of the stress control method is flexible, which is more in line with the site conditions. In this test, the flexible latex membrane was used to simulate slurry film on the tunnel excavation face and the slurry support pressure was performed by water pressure.

The model test system consists of a rectangular model container for the preparation of the sand layer, a flexible pressure chamber, a water tank and a dynamic measurement system. The size of the acrylic container is 600 mm × 600 mm × 650 mm, with wall thickness of 20 mm as shown in Fig. 1. A series of steel frames was used to reinforce the container's lateral surfaces. Considering the symmetry of a circular tunnel, a semi-tunnel shell model with 150 mm in diameter D, 200 mm in length and 4 mm in thickness were designed. The front of shield shell is covered by a semi-cylindrical flexible latex membrane with 0.5 mm in thickness and 3 cm in length, which is of negligible strength. The shield shell and latex membrane form a flexible pressure chamber which is connected to the water tank outside the model container through the inlet pipe. Photographs of the model test apparatus is shown in Fig. 2. In the model test, the diameter of the shield model is 150 mm, corresponding to 15 m of the prototype, i.e. the similarity scale adopted is 1:100.

In order to accurately control the decrease rate of the water

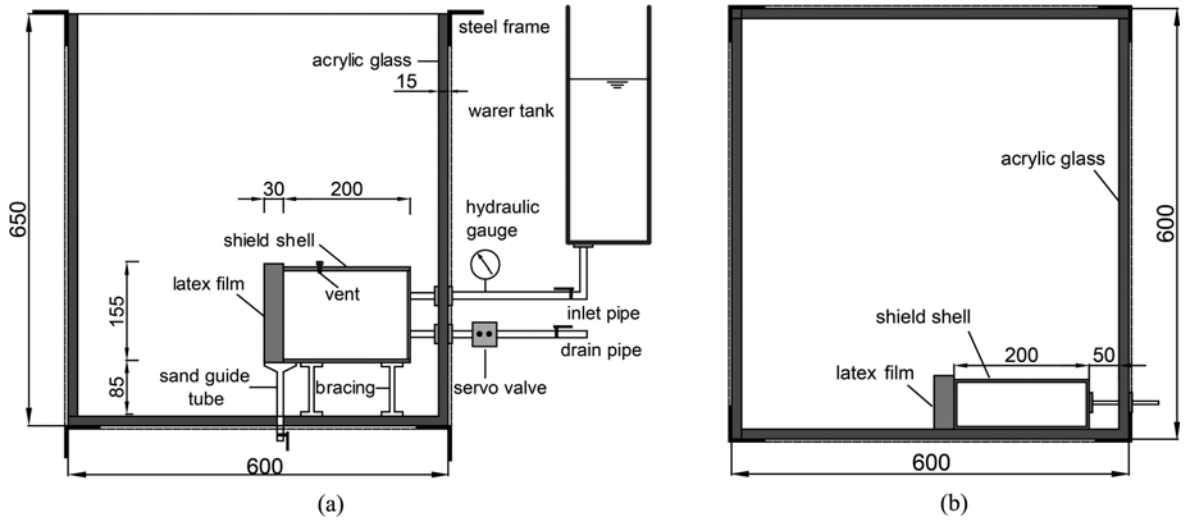

Fig. 1. Schematic Diagrams of the Test Configuration (dimensions in mm): (a) Front View, (b) Above View

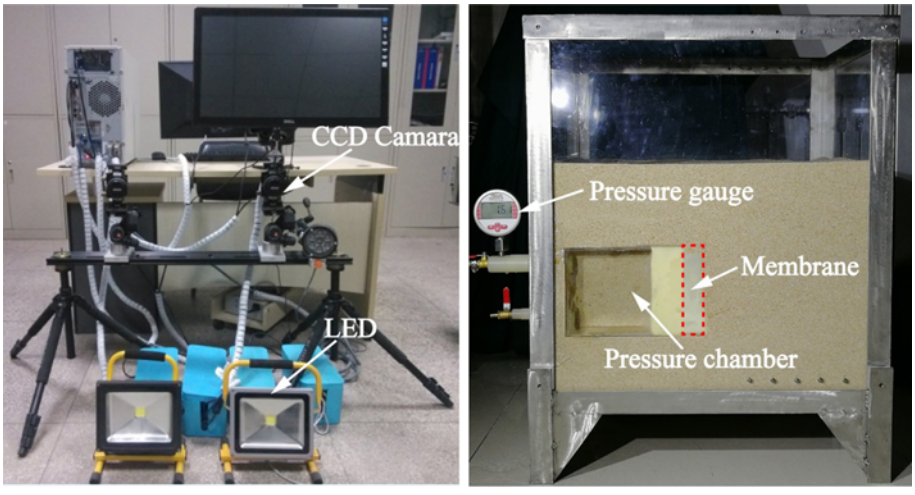

Fig. 2. Photographs of the Model Test Apparatus: (a) PIV Hardware System, (b) Model Container

pressure in the flexible chamber, a servo valve was provided on the drain pipe, which can control the support pressure by stabilize the rate of flow. During the tests, the support pressure in flexible water chamber was measured by a water pressure gauge which can achieve pressure from -5 kPa to 10 kPa with an accuracy of 0.001 kPa. The soil behavior around the tunnel excavation face was measured by DIC technique (White et al., 2003). The relative displacement between two images can be achieved by the software GeoPIV. The accuracy of DIC measurement is affected by many factors, such as image speckle, imaging equipment, image processing algorithm, image shooting environment, etc. In this paper, the iterative grid-refining algorithm was applied to increase the accuracy of GeoPIV (White et al., 2003; Stanier et al., 2015; Take, 2015; Ni et al., 2018). The algorithm permitted measuring soil deformation with a resolution of 0.1 pixels corresponding to 0.01 – 0.02 mm in this paper.

2.2 Model Test Materials

Chinese Xiamen ISO standard sand was used in the model tests. Hand tamping technique was conducted for the preparation of sand with different initial densities. Loose sand was prepared by carefully putting the sand into the container, avoiding any compacting action. As for medium dense sand, hand tamping was conducted with the certain compaction energy at an interval of 5 cm to reach the target relative density. The dense sand was compact once at an interval of 3 cm. After laying the stratum, the sand was stabilized under the action of gravity for 24 hours. Sand direct shear tests were conducted for different initial densities. The physical properties and friction angle of the sand at the critical state are shown in Table 1.

An effective friction treatment system can help to eliminate the boundary effect, such as double layered polyethylene sheets with silicone grease in between (Ni et al., 2018). Tognon et al. (1999) discussed different techniques to reduce the friction angle

Table 1. Parameters of Sand in Model Test

Type	Loose sand	Medium dense sand	Dense sand
Coefficient of uniformity C_u	1.40	1.40	1.40
Mean grain size d_{50} (mm)	0.78	0.78	0.78
Effective grain size d_{10} (mm)	0.57	0.57	0.57
Maximum dry density $\rho_{d\max}$ (g/cm^3)	1.70	1.70	1.70
Minimum dry density $\rho_{d\min}$ (g/cm^3)	1.41	1.41	1.41
Dry density ρ_d (g/cm^3)	1.46 – 1.49	1.52 – 1.57	1.59 – 1.61
Initial relative density D_r (%)	23 – 32	46 – 59	68 – 73
Internal friction angle φ (°)	29.7	34.3	38.4

at sidewalls, and pointed out that it is necessary to implement friction treatment for laboratory tests, especially for small-scale tests. In this paper, lubricating grease was used to reduce the friction between acrylic and sand.

2.3 Test Procedure

Different tests for three shield cover depths (C/D=0.5, 1.0, 2.0) and three densities of sand stratum were conducted. Stress control method was adopted in nine groups of tests to realize the failure of excavation face. The entire testing program is summarized in Table 2 and the specific steps for a single test are listed below:

1. Before the tests, the tunnel excavation face was kept in stable and the slurry pressure in the flexible water chamber was set equal to the horizontal earth pressure on the face during the sand layer preparation.
2. Charge coupled device (CCD) camera was set at the front window of the container and the light emitting diode (LED) light was placed in proper place.
3. Before image shooting, the camera was calibrated. A series of camera shooting indexes was achieved, so that there was high precision for the camera shooting.
4. Drain valve was turned on for the discharge of the water and water pressure in flexible chamber was monitored and recorded in real time. The frame rate of the camera is set at 1 frame every 30 second.
5. The test was terminated until an apparent settlement trough appeared on the ground surface.

Table 2. Summary of Laboratory Test Program

Test number	Condition	Density degree	C/D
A1	Dry	Loose	0.5
A1	Dry	Loose	1.0
A1	Dry	Loose	2.0
B1	Dry	Medium Dense	0.5
B1	Dry	Medium Dense	1.0
B1	Dry	Medium Dense	2.0
C1	Dry	Dense	0.5
C1	Dry	Dense	1.0
C1	Dry	Dense	2.0

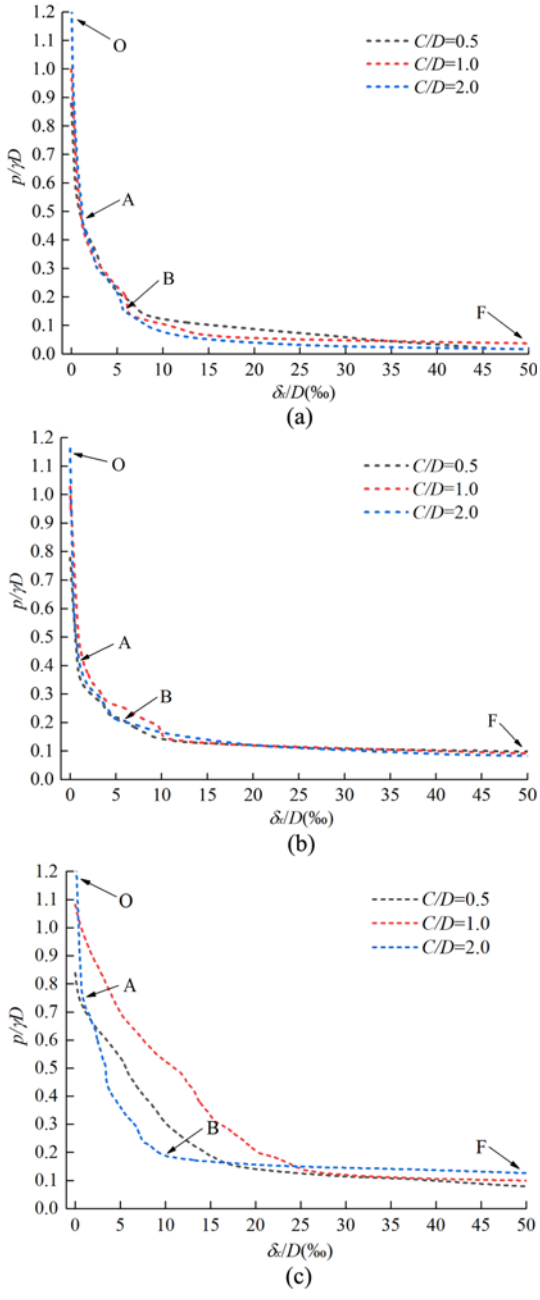

Fig. 3. Normalized Support Pressure–Horizontal Displacement Curves of Model Tests: (a) Dense Sand, (b) Medium Dense Sand, (c) Loose Sand

3. Experimental Results and Discussions

3.1 Failure Process

Figure 3 shows the curves of support pressure vs horizontal displacement of excavation face for different dense degree. The normalized horizontal displacement of tunnel center δ_x/D is on the transverse axis, and the normalized support pressure $p/\gamma D$ is on the longitudinal axis. In Fig. 3, δ_x is the displacement of the face center, p is support pressure, γ is the bulk density of dry sand. In relation to the support pressure, the face displacement can be divided into three stages: First stage (O−A): In this stage, negligible deformations were observed (less than 0.1% of shield diameter). With the decrease of support pressure, the displacement is almost linear with the normalized support pressure. Second stage (A−B): In this stage, the excavation face appeared small local instability deformation. With the decrease of support pressure, the increase rate of excavation face displacement increases gradually. The critical failure point of excavation face is found at point B. Third stage (B−F): The excavation face has been failed with overall instability in this stage. Although the support pressure hardly changes, the face deformation increases sharply.

The shapes of curves under three burial depths are similar for dense sand stratum state (Fig. 3(a)). The displacement corresponding to point A is less than 0.1% of the tunnel diameter, while displacement at point B is 0.62% to 1.19% of it. With the burial depth increased, the support pressure corresponding to point B decreases gradually and the displacement increases. The curves for medium dense sand stratum are similar to those in dense sand stratum (Fig. 3(b)), but the support pressures and horizontal displacements corresponding to point B are larger than those in dense sand stratum under the same burial depth. The curves for loose sand stratum differ greatly from other two densities of stratum, which are manifested in shorter elastic stage and longer local failure stage (Fig. 3(c)).

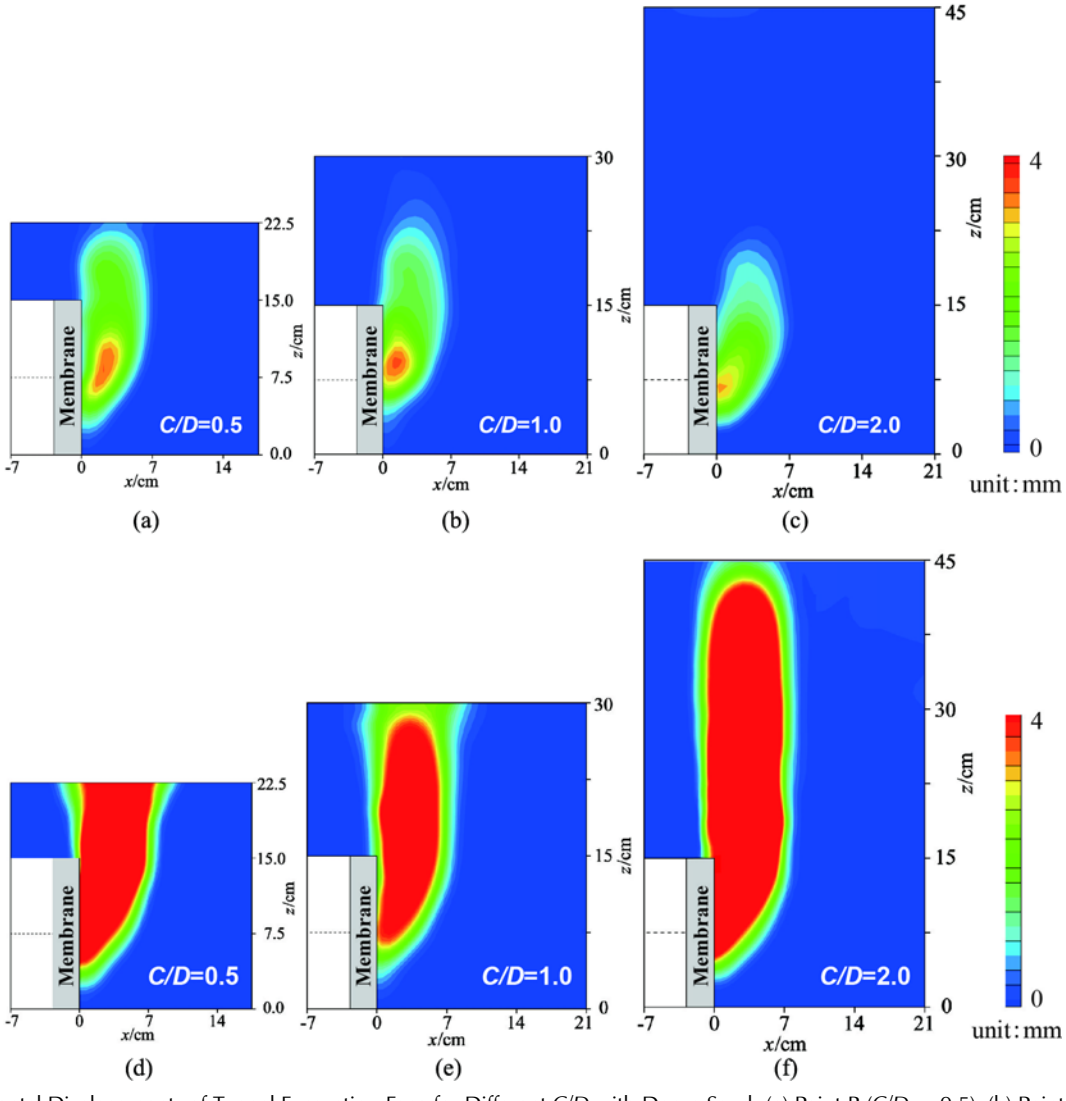

Fig. 4. Incremental Displacements of Tunnel Excavation Face for Different C/D with Dense Sand: (a) Point B (C/D = 0.5), (b) Point B (C/D = 1.0), (c) Point B (C/D = 2.0), (d) Point F (C/D = 0.5), (e) Point F (C/D = 1.0), (f) Point F (C/D = 2.0)

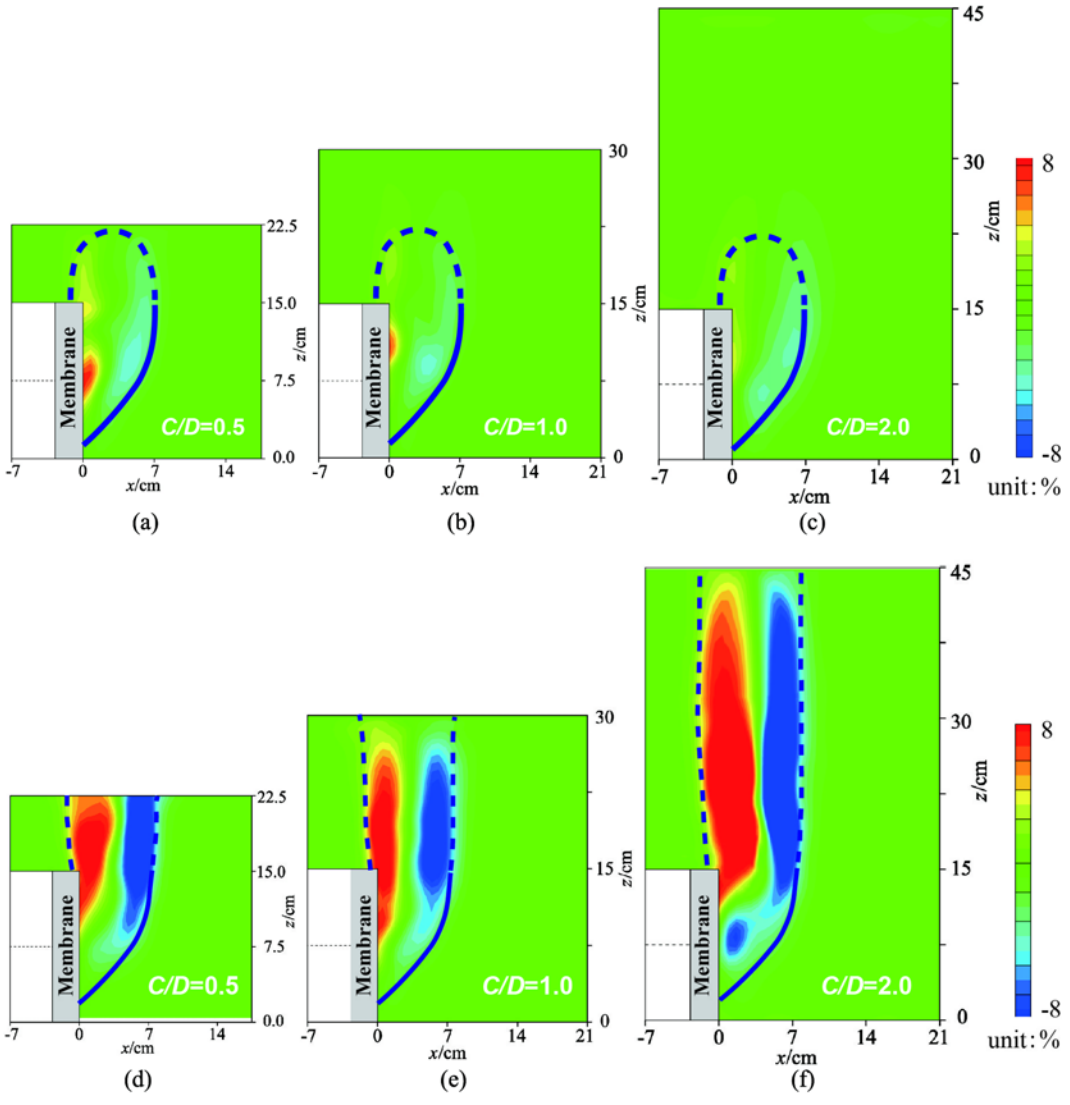

Fig. 5. Incremental Shear Strains of Tunnel Excavation Face for Different *C*/*D* with Dense Sand: (a) Point B (*C*/*D* = 0.5), (b) Point B (*C*/*D* = 1.0), (c) Point B (*C*/*D* = 2.0), (d) Point F (*C*/*D* = 0.5), (e) Point F (*C*/*D* = 1.0), (f) Point F (*C*/*D* = 2.0)

3.2 Soil Deformation

Incremental displacements and shear strains of tunnel excavation face for different *C*/*D* with dense sand are shown in Fig. 4 and Fig. 5, respectively. Point B is the critical failure point for the overall instability failure of excavation face and point F is the final failure point of excavation face. In the critical failure

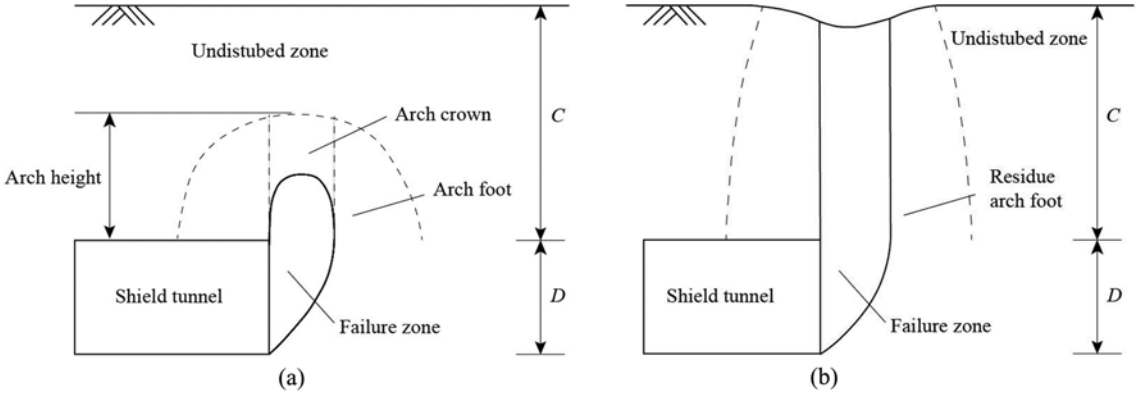

Fig. 6. Schematic Diagram of Soil Arching Effect on Shield Excavation Face: (a) Local Collapse, (b) Global Collapse

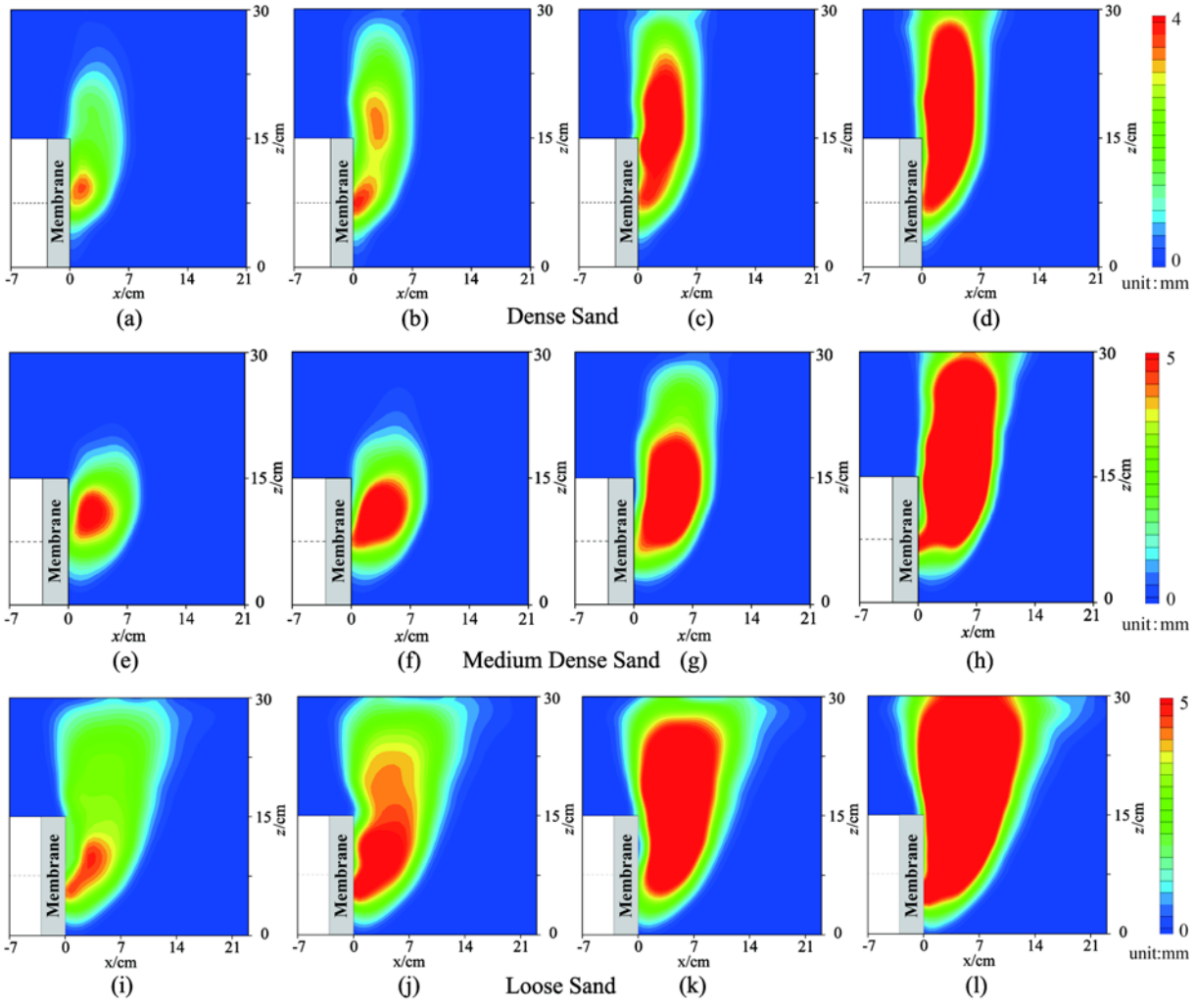

Fig. 7. Displacement Field of Tunnel Excavation Face for Different D_r with C/D = 1.0: (a) Dense Sand ($p/\gamma D$ = 0.121), (b) Dense Sand ($p/\gamma D$ = 0.105), (c) Dense Sand ($p/\gamma D$ = 0.071), (d) Dense Sand ($p/\gamma D$ = 0.035), (e) Medium Dense Sand ($p/\gamma D$ = 0.138), (f) Medium Dense Sand ($p/\gamma D$ = 0.126), (g) Medium Dense Sand ($p/\gamma D$ = 0.103), (h) Medium Dense Sand ($p/\gamma D$ = 0.072), (i) Loose Sand ($p/\gamma D$ = 0.165), (j) Loose Sand ($p/\gamma D$ = 0.126), (k) Loose Sand ($p/\gamma D$ = 0.106), (l) Loose Sand ($p/\gamma D$ = 0.081)

condition (point B), the soil deformation has extended to the ground surface when C/D = 0.5. However, due to the soil arch above the tunnel crown, the soil deformation did not penetrate the ground when C/D = 1.0 and 2.0. As shown in Fig. 6(a), the soil arch crown and arch foot were formed above and around the failure zone. With the reduction of support pressure, the failure zone extended to the ground surface, causing the original soil arch zone to be damaged and further developed to the ground surface until no soil arch was formed when the failure zone also penetrated the ground surface, as is shown in Fig. 6(b). It is obvious that the failure mode at point F is composed of a wedge-shaped slip surface in front of the tunnel and a prism chimney above. It can be seen from Figs. 4 and 5 that the influence of C/D can be neglected, this conclusion is consistent with the results obtained by Chambon and Corté (1994).

Incremental displacements and shear strains of tunnel excavation face for different densities with C/D=1.0 are shown in Figs. 7 and 8, respectively. It can be seen that initial density of stratum has a great influence on soil deformation. For dense and medium dense condition, soil deformation mainly appeared near the tunnel excavation face. With the decrease of support pressure, soil deformation gradually extended to the ground surface and finally formed the shape consisted of a wedge and a prism chimney above (Figs. 8(a) to 8(d)). The failure shape is similar to the failure mode proposed by Horn (1961). However, the dip angle of the upper wedge and the width of the upper prism in the failure mode for medium dense sand are larger than those for dense condition (Figs. 8(e) to 8(h)).

The failure mode in loose sand is a relatively dispersed failure zone, i.e. a "trumpet" shape extending to the ground surface in the direction of excavation face (Figs. 8(i) to 8(l)), which is completely different from that in dense and medium dense sand stratum. Because the internal friction angles of medium dense and loose sand are relatively small and the contacts between sand

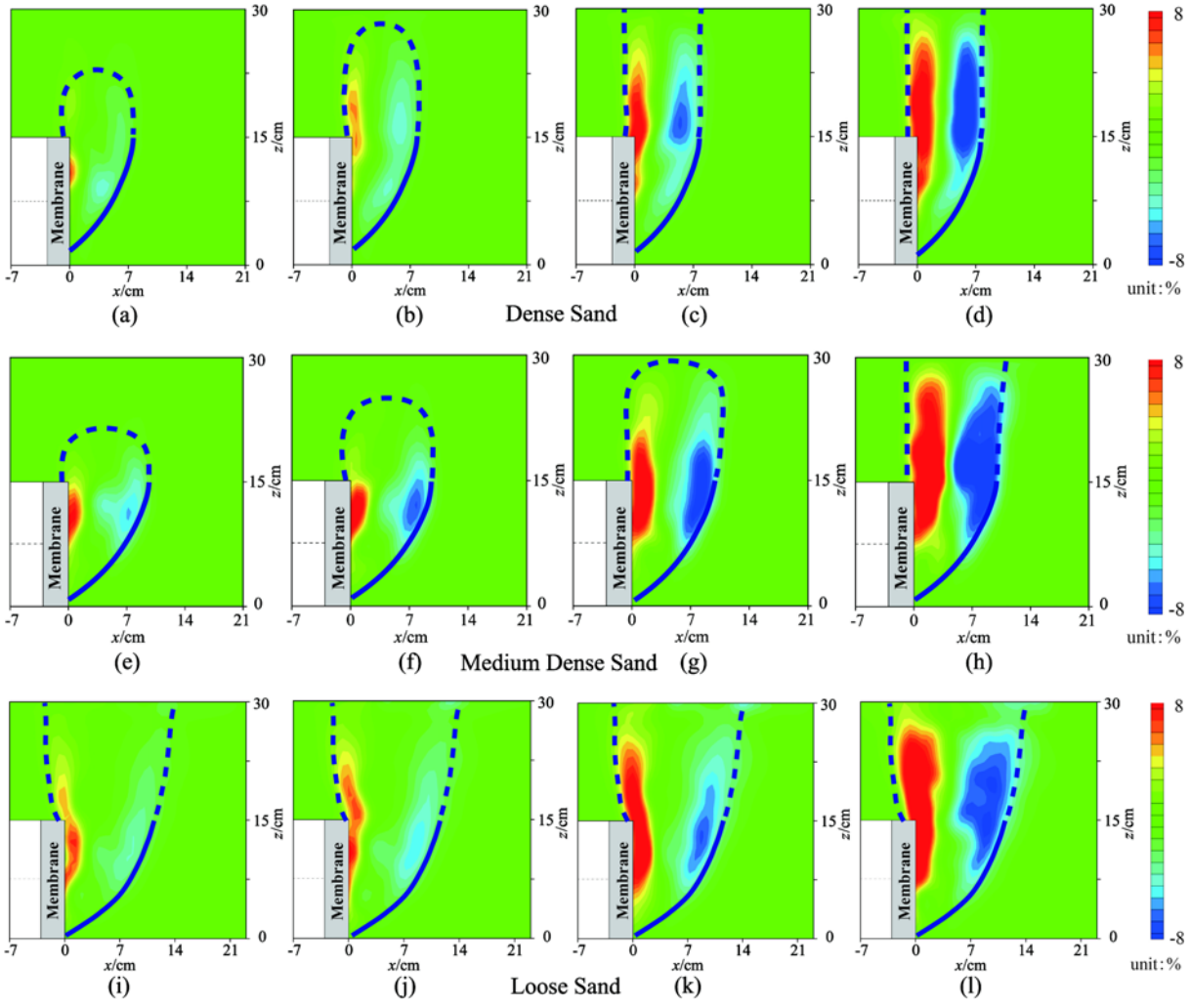

Fig. 8. Incremental Shear Strains of Tunnel Excavation Face for Different D_r with C/D = 1.0: (a) Dense Sand ($p/\gamma D$ = 0.121), (b) Dense Sand ($p/\gamma D$ = 0.105), (c) Dense Sand ($p/\gamma D$ = 0.071), (d) Dense Sand ($p/\gamma D$ = 0.035), (e) Medium Dense Sand ($p/\gamma D$ = 0.138), (f) Medium Dense Sand ($p/\gamma D$ = 0.126), (g) Medium Dense Sand ($p/\gamma D$ = 0.103), (h) Medium Dense Sand ($p/\gamma D$ = 0.072), (i) Loose Sand ($p/\gamma D$ = 0.165), (j) Loose Sand ($p/\gamma D$ = 0.126), (k) Loose Sand ($p/\gamma D$ = 0.106), (l) Loose Sand ($p/\gamma D$ = 0.081)

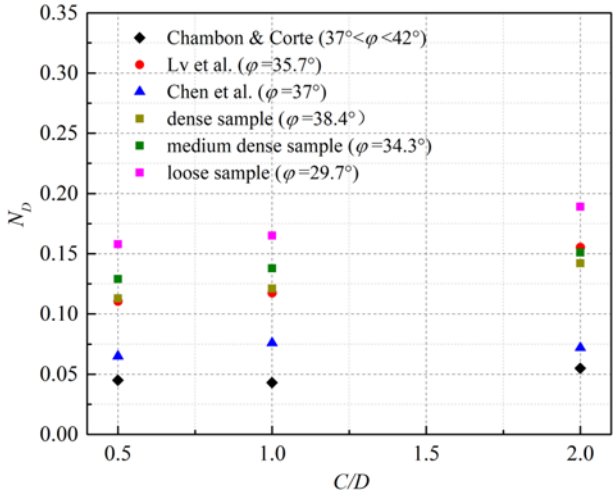

Fig. 9. Limit Support Pressure of Excavation Face in Dry Sand

particles are not close enough, the stress on the sand above the excavation face is larger than its own shear strength, resulting in the overall shear displacement and a large failure zone under the action of gravity.

3.3 Limit Support Pressure

The limit support pressure p_f obtained by experiment in this paper is compared with the results achieved by other investigators, as shown in Fig. 9, where $N_D = p_f/\gamma D$ is the normalized limit support pressure of excavation face. It can be inferred from Fig. 9 that burial depth and initial density have a great influence on N_D, i.e., N_D increases with C/D and decreases with initial density. It can be also obviously seen in Fig. 9 that the limit support pressure obtained by the model tests in dense and medium dense sand in this paper is close to the result obtained by Lv et al. The results obtained by Chen et al. and Chambon and Corté are far less than those obtained by the model tests in this paper. That

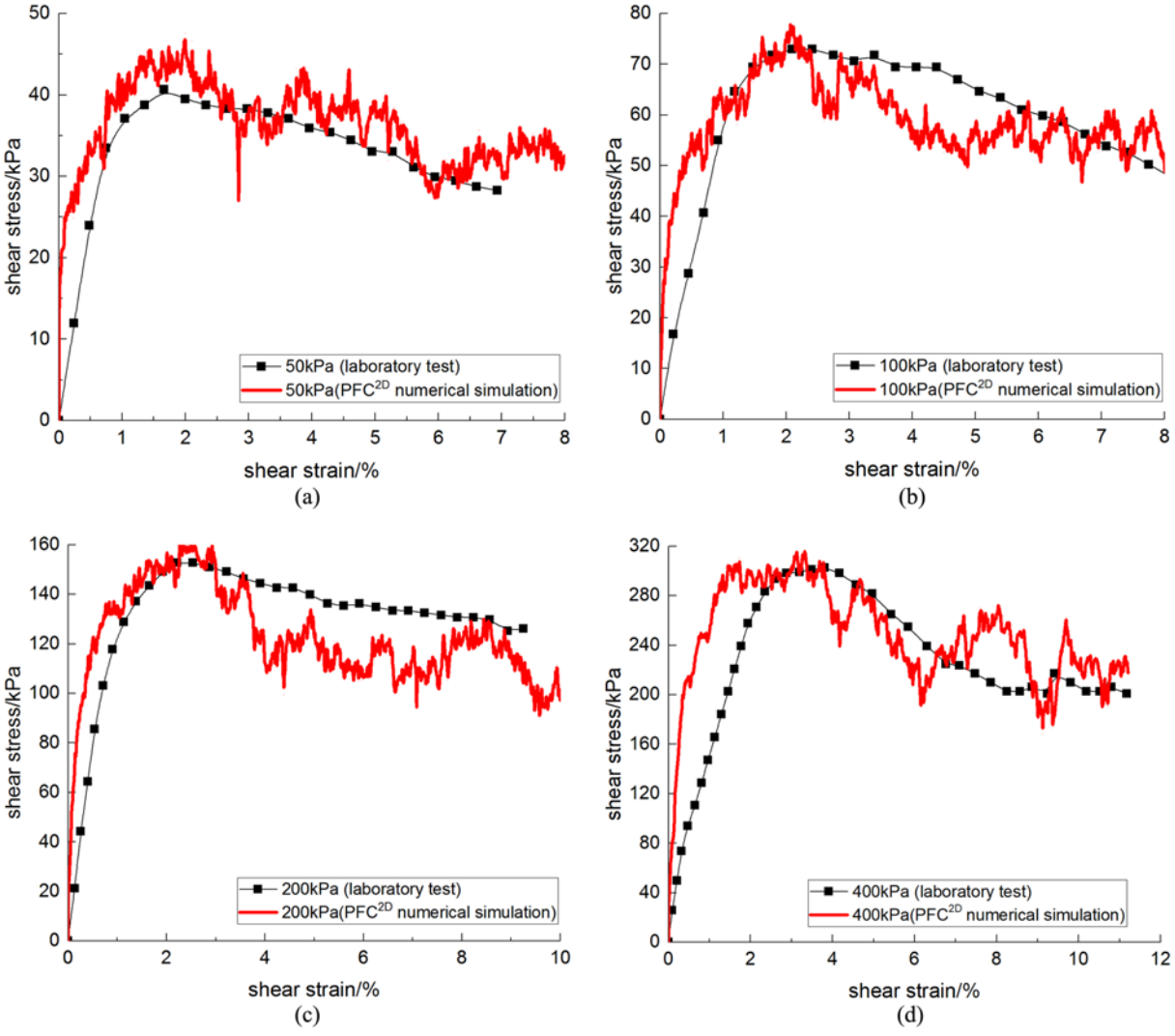

Fig. 10. Stress-Strain Curves for Sand of Laboratory Tests and PFC^{2D} Simulations: (a) σ_3 = 50 kPa, (b) σ_3 = 100 kPa, (c) σ_3 = 200 kPa, (d) σ_3 = 400 kPa

may be due to the displacement control method adopted by Chen et al. to achieve the face failure. Besides, the sand used by Chambon and Corté contained a certain cohesion.

4. PFC^{2D} Analysis

4.1 Numerical Setup

4.1.1 Parameters

PFC^{2D} was used to simulate the model test. The basic principle of PFC is derived from molecular dynamics and it is a tool for studying the mechanical characteristics and behavior of medium through the perspective of micro-structure (Cundall and Strack, 1979). PFC model mainly consists of discs or balls, walls are used to impose boundary constraints. Different from continuum simulation, in the numerical calculation of PFC^{2D}, it is necessary to determine the parameters reflecting the microscopic characteristics of soil materials. Through numerical biaxial tests, the matching of microscopic parameters and macroscopic parameters was realized.

Table 3. The Numerical Parameters of PFC^{2D} Model

Normal contact stiffness K_n (N/m)	Tangential contact stiffness K_s (N/m)	Particle friction parameter f	Particle density ρ_s (kg/m^3)
2×10^6	2×10^6	0.85	2,630

Linear contact model was used to simulate sand material and sand microscopic parameters were calibrated by biaxial tests. Considering the shield burial depth, the normal stresses σ_3 were set to be 50, 100, 200 and 400 kPa, respectively. Fig. 10 shows the stress-strain curves for dense sand specimen of laboratory tests and PFC^{2D} simulations. The results of numerical simulation and laboratory tests have an excellent correlation, indicating that model microscopic parameters are appropriate for simulating the actual sand in physical model test. The microscopic parameters adopted for the PFC^{2D} model are listed in Table 3.

During the PFC simulation, the boundary walls and shield

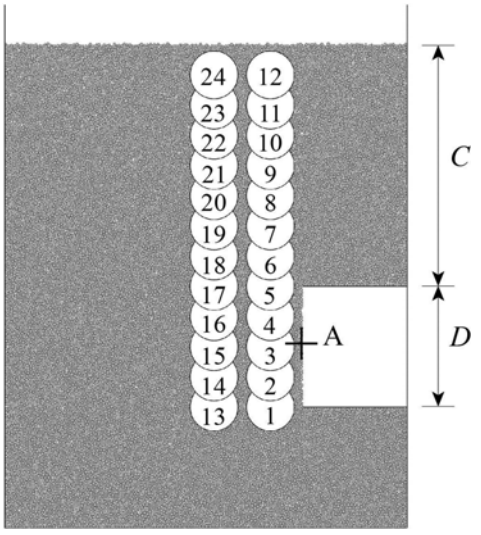

Fig. 11. Distribution of Measuring Circles and Monitoring Points (C/D=2.0)

shell in the model container were simulated by "Wall" command since they are rigid material. Normal and tangential stiffness of the wall were set to be 2×10^8 N/m. In order to simulate the surface roughness of the wall in the model container, a small friction coefficient of 0.2 was set to the wall during the simulation. The dimensions of numerical model were set to be the same with the physical model.

4.1.2 Modeling of Shield Tunnel

The establishment of PFC model involves three steps. Firstly, the particles were generated according to the sand in experiment and two-dimensional porosity achieved by the three-dimensional porosity. By controlling the particles numbers, three densities of sand stratum were performed. Secondly, the velocity field and displacement field of the whole calculation model were set to be zero. Sand in excavation zone was deleted and the shield shell was established. Finally, the wall on excavation face was removed and the support stress equal to the horizontal earth pressure was applied on excavation face. The static equilibrium state of excavation face was reached by iteration calculation.

4.1.3 Failure Simulation and Monitor Points

Stress control method was used to simulate the failure process. In particle flow simulation, it is considered as the beginning of failure, where for the first time of considerable value of unbalanced force and large displacement occurred without decreasing the support pressure were observed.

In order to obtain the failure mechanism of excavation face, soil deformation, earth pressure and porosity were monitored during the simulation process. Soil deformations were obtained by monitoring the ball displacements. Besides, earth pressure and porosity in the stratum were obtained by the measuring circles. The layout of particle deformation monitoring points and measuring circles are shown in Fig. 11, where 1 – 24 are the numbers of measuring circles and point A is the monitoring point of horizontal displacement at the excavation face center.

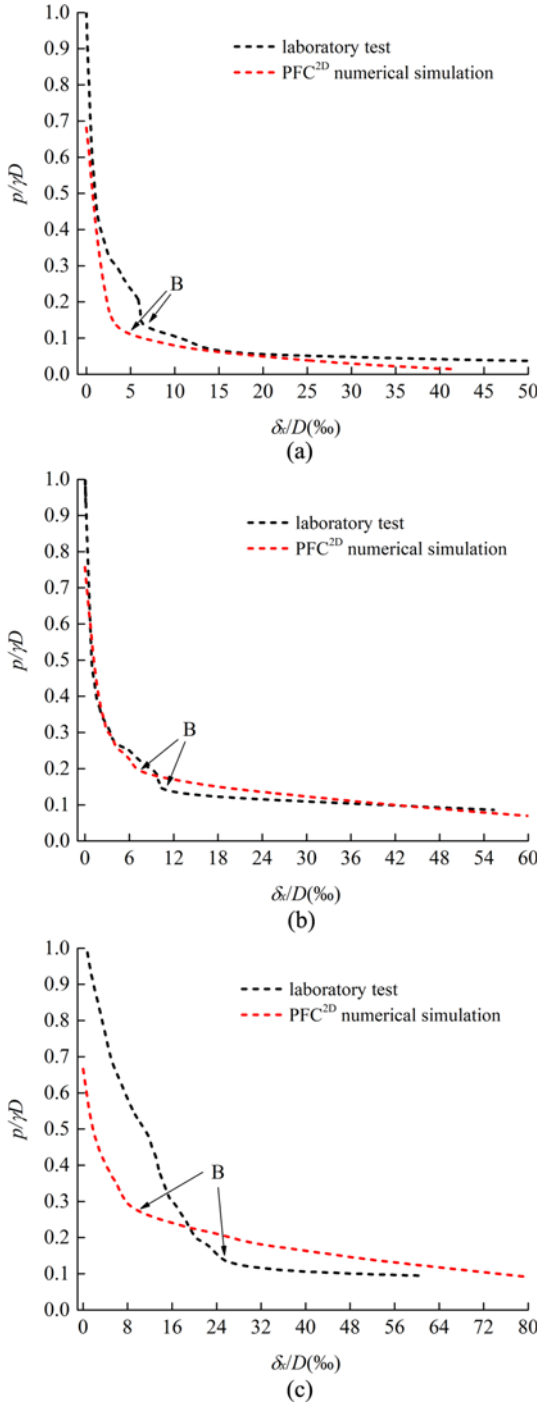

Fig. 12. Normalized Support Pressure–Horizontal Displacement Curves of Laboratory Tests and PFC^{2D} (C/D = 1.0): (a) Dense Sand, (b) Medium Dense Sand, (c) Loose Sand

4.2 PFC^{2D} Simulation Results

4.2.1 Failure Process

Figure 12 shows face displacement δ_x versus the normalized

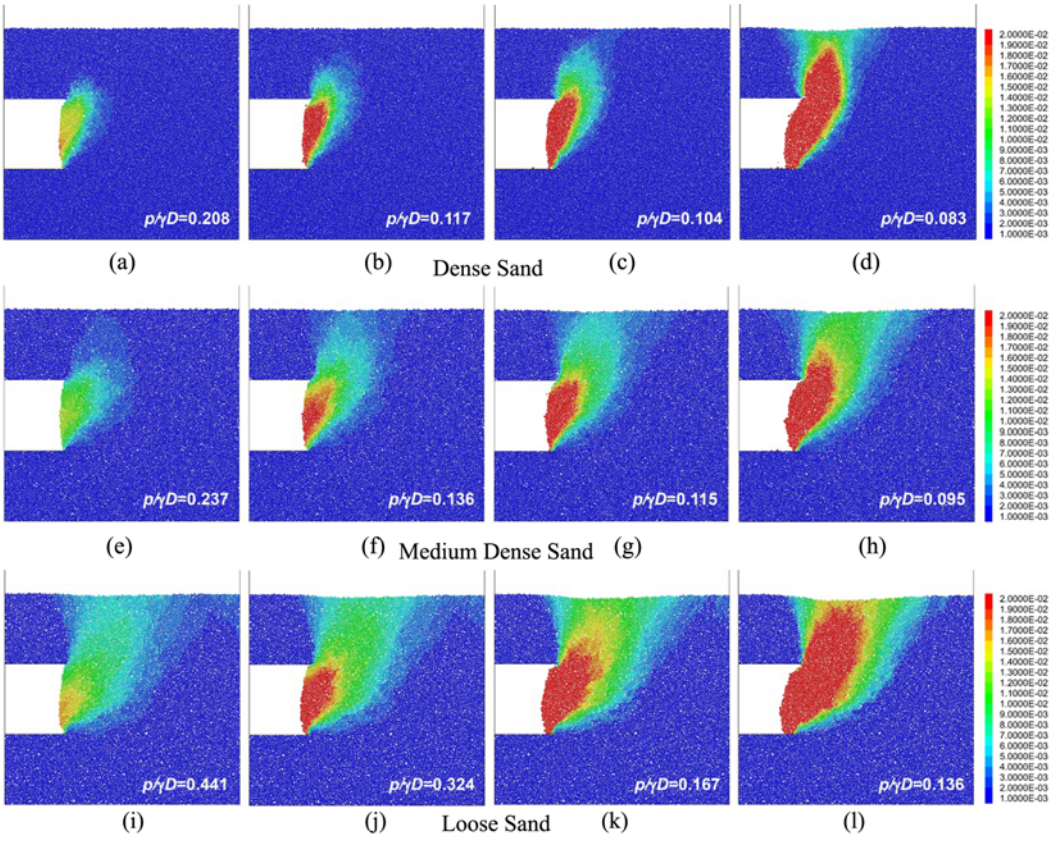

Fig. 13. Soil Deformation of PFC^{2D} for Different Initial Densities (unit: mm): (a) Dense Sand ($p/\gamma D = 0.208$), (b) Dense Sand ($p/\gamma D = 0.117$), (c) Dense Sand ($p/\gamma D = 0.104$), (d) Dense Sand ($p/\gamma D = 0.083$), (e) Medium Dense Sand ($p/\gamma D = 0.237$), (f) Medium Dense Sand ($p/\gamma D = 0.136$), (g) Medium Dense Sand ($p/\gamma D = 0.115$), (h) Medium Dense Sand ($p/\gamma D = 0.095$), (i) Loose Sand ($p/\gamma D = 0.441$), (j) Loose Sand ($p/\gamma D = 0.324$), (k) Loose Sand ($p/\gamma D = 0.167$), (l) Loose Sand ($p/\gamma D = 0.136$)

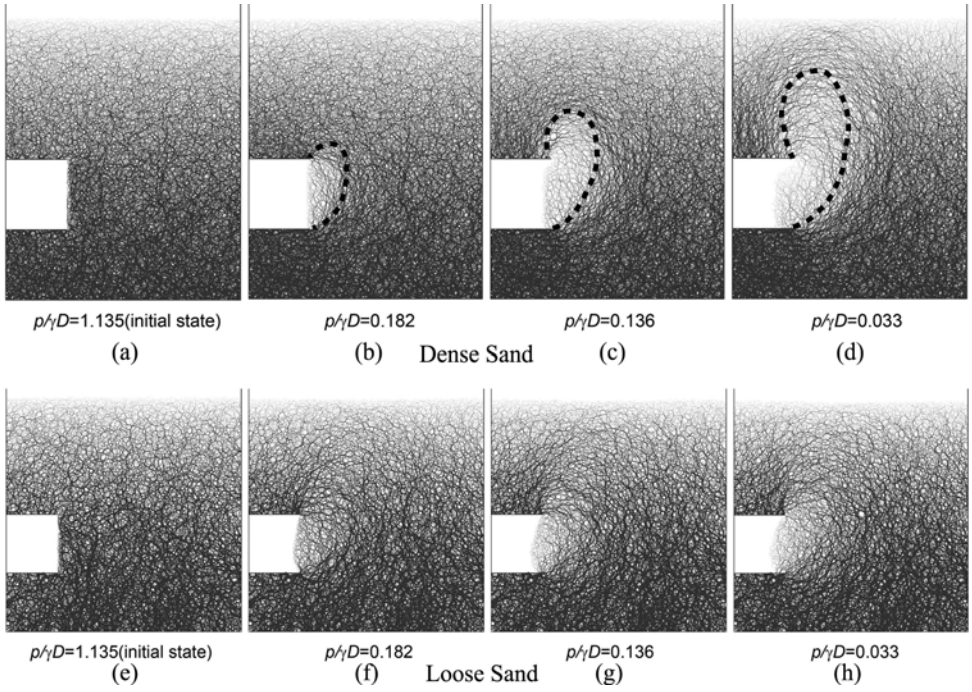

Fig. 14. Distribution of Contact Force for $C/D = 2.0$: (a) Dense Sand ($p/\gamma D = 1.135$ (initial state)), (b) Dense Sand ($p/\gamma D = 0.182$), (c) Dense Sand ($p/\gamma D = 0.136$), (d) Dense Sand ($p/\gamma D = 0.033$), (e) Loose Sand ($p/\gamma D = 1.135$ (initial state)), (f) Loose Sand ($p/\gamma D = 0.182$), (g) Loose Sand ($p/\gamma D = 0.136$), (h) Loose Sand ($p/\gamma D = 0.033$)

support pressure $p/\gamma D$ for different densities stratum when C/D=1.0. It is obvious that the normalized support pressure–displacement curves of PFC^{2D} are consistent with the observations in model tests.

The developments of displacement field with different densities are shown in Fig. 13. As the support pressure decreased, the failure zone extended to the tunnel crown and the initial failure boundary was formed when the failure zone in the soil was arched above the excavation face, which is consistent with the observation in model tests. The deformation process in medium dense sand stratum was similar to that in dense sand. The failure mode in loose sand stratum is "trumpet" shaped extending from the excavation face to the ground surface, which is consistent with the observations in model tests.

4.2.2 Soil Arching Effect

Soil arching effect can significantly improve the stability of tunnel so the evolution process of contact force chain and earth pressure for C/D = 2.0 were studied.

The soil contact force chain on the excavation face can directly reflect the soil arching effect. In Fig. 14, the dark grey solid lines represent the force chain and the thickness of the force chain represents the particle contact force. For dense condition, the weak force chain is mainly appeared in front of the excavation face, while the strong arch-like chain is formed above the tunnel crown, as is shown in Figs. 14(a) to 14(d). The reason for this phenomenon is that, with the decrease of support pressure, the dislocation of soil particles in front of the excavation face results in the deflection of the original large vertical principal stress axis of the particles, forming a soil arch which is conducive to transmit sand gravity. That made part of excavation face in the soil arch area in the relatively small stress state. With the continuous decrease of support pressure, the boundary of weak force chain in front of excavation face and failure zone gradually extended to the ground surface, which means the soil arch disappeared completely. It can be inferred from Figs. 14(e) – 14(h) that compared with dense sand, the soil arching effect is not obvious for loose condition.

Figure 15 shows the distribution law of earth pressure on excavation face for dense condition. As shown in Fig. 15(a), the vertical earth pressure increases almost linearly with the burial depth in the initial state. From the initial state to the critical failure point (point B), the vertical earth pressure from the bottom of tunnel to 0.5D above the tunnel crown dramatic decreases, but remains almost invariant above it. In contrast, the horizontal earth pressure decreases sharply in the range from the bottom of tunnel to 0.2D above the tunnel crown, but increases slightly in the range from 0.2D to 1.0D above the tunnel crown, as is shown in Fig. 15(b). It can be inferred that the soil arch occurs in the range from 0.5D to 1.0D above tunnel crown.

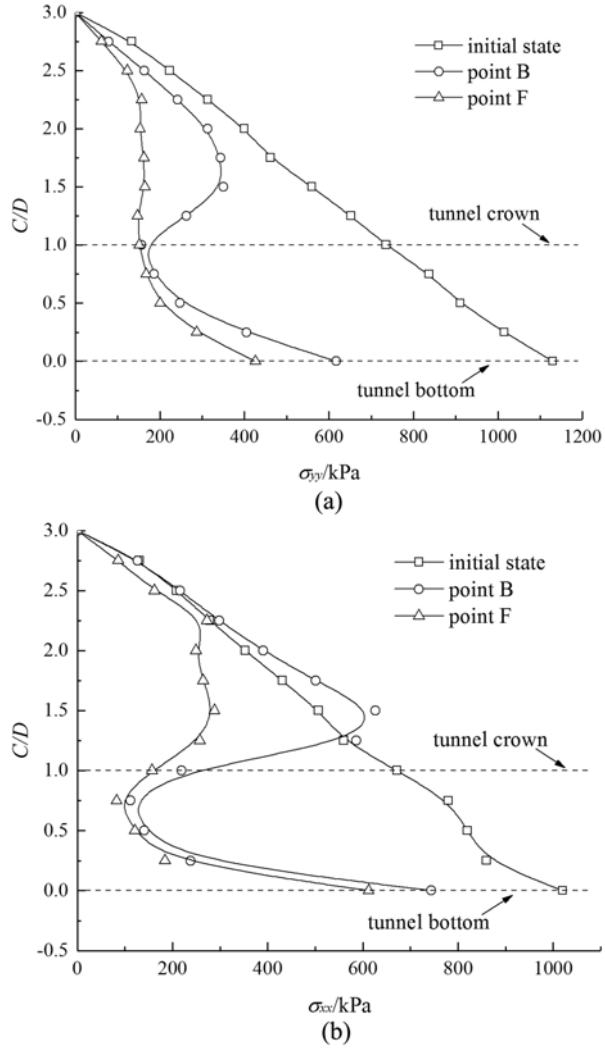

Fig. 15. Variation of Stress on Tunnel Excavation Face for Dense Sand with C/D = 2.0: (a) Vertical Stress along Depth, (b) Horizontal Stress along Depth

4.2.3 Limit Support Pressure

The limit support pressures calculated by PFC^{2D} are shown in Table 4. It is obvious that N_D increases with the burial depth and decreases with initial density, which is consistent with the observations in model tests. But there are more or less differences for N_D values: the results of particle flow simulation are less for

Table 4. Comparison of Limit Support Pressure

Initial density (g/cm^3)	C/D	N_D for physical tests	N_D for PFC^{2D} simulation	N_D for limit analysis
1.60	0.5	0.113	0.093	0.117
	1.0	0.121	0.100	0.117
	2.0	0.142	0.115	0.117
1.55	0.5	0.129	0.132	0.136
	1.0	0.138	0.143	0.136
	2.0	0.151	0.151	0.136
1.48	0.5	0.158	0.224	0.167
	1.0	0.165	0.243	0.167
	2.0	0.189	0.252	0.167

dense sand and larger for loose condition, while the values for medium dense condition are very close. That may be related to the selection of particle shape and microscopic parameters in PFC simulation. While the macroscopic parameters of sand are calibrated by numerical direct shear tests, it is difficult to accurately obtain the failure of excavation face for different densities which is identical with the actual state. However, the overall law is consistent with the test results, which also shows the feasibility to simulating the failure of shield excavation face in sand stratum by PFC.

The formula proposed by Leca and Dormieux (1990) was adopted as follows:

$$\sigma_t = \gamma D N_\gamma + c N_c + \sigma_s N_s \,, \tag{1}$$

where N_g, N_c and N_s are dimensionless parameters, representing the influence factors of overlying soil layer, cohesion and overload on the limit support pressure, respectively.

The theoretical calculation results of N_D are shown in Table 4. It can be inferred that the upper-bound solutions are independent with the burial depth, but N_D decreases gradually with density, which is different from the observations in model tests and numerical calculation. When C/D = 0.5, the upper bound limit method overestimates N_D. As to C/D = 2.0, the N_D values are underestimated, when it is unreasonable to use this method to evaluate the stability of excavation face.

5. Conclusions

Based on model test and PFC analysis, failure mechanism of face for slurry shield-driven tunnel in sand was investigated. Soil deformation, failure mode and soil arching effect of excavation face in dry sand stratum for different densities and burial depths were revealed. The main conclusions are as follows:

1. With the decrease of support pressure, there are three stages for the excavation face deformation. In the first stage, quite small face deformations were observed. The excavation face appeared small local instability deformation in the second stage, and the face displacement increased sharply with hardly decrease of support pressure in the last stage. The support pressure–displacement curves in loose sand differ greatly from other two densities, which are manifested in shorter elastic stage and longer local failure stage.
2. The cover depth has a negligible effect on the failure mode of excavation face, which is consistent with the results obtained by Chambon, while the initial density of stratum has a great influence on the soil deformation. The failure shape in dense sand stratum is a combination of a wedge with slip arc and a prism chimney above. However, the failure mode in loose sand stratum is a relatively dispersed "trumpet" shape failure zone.
3. During the failure process of slurry shield tunnel excavation face, soil arch was formed in the upper part of the failure zone. The distribution of particle force chain and earth pressure in the stratum can reflect the soil arching effect of excavation face.
4. The limit support pressure increases with the burial depth and decreases with the compactness, which can be verified by the observations in model tests and PFC calculations.

Acknowledgments

This work was financially supported by the National High-tech R&D Program (863 Program) (through grant No. 2012AA041802) and the Doctoral Student Innovation Foundation of NCWU.

ORCID

Not Applicable

References

Ahmed M, Iskander M (2012) Evaluation of tunnel face stability by transparent soil models. *Tunnelling and Underground Space Technology* 27(1):101-110, DOI: 10.1016/j.tust.2011.08.001

Anagnostou G, Kovári K (1994) The face stability of slurry shield-driven tunnels. *Tunneling and Underground Space Technology* 9(2):165-174, DOI: 10.1016/0886-7798(94)90028-0

Anagnostou G, Kovári K (1996) Face stability conditions with earth-pressure-balanced shields. *Tunnelling and Underground Space Technology* 11(2):165-173, DOI: 10.1016/0886-7798(96)00017-X

Broere W, van Tol AF (2000) Influence of infiltration and groundwater flow on tunnel face stability. In: Kusakabe O, Fujita K, Miyazaki Y (eds) Geotechnical aspects of underground construction in soft ground. Balkema, Rotterdam, 339-344

Chambon P, Corté JF (1994) Shallow tunnels in cohesionless soil: Stability of tunnel face. *Journal of Geotechnical Engineering* 120(7): 1148-1165, DOI: 10.1061/(ASCE)0733-9410(1994)120:7(1148)

Chen RP, Li J, Kong LG, Tang LJ (2013) Experimental study on face instability of shield tunnel in sand. *Tunnelling and Underground Space Technology* 33(1):12-21, DOI: 10.1016/j.tust.2012.08.001

Chen RP, Tang LJ, Ling DS, Chen YM (2011) Face stability analysis of Shallow shield tunnels in dry sandy ground using the discrete element method. *Computers & Geotechnics* 38(2):187-195, DOI: 10.1016/j.compgeo.2010.11.003

Cundall PA, Strack O (1979) A discrete numerical model for granular assemblies. *Géotechnique* 29(1):47-65, DOI: 10.1680/geot.1980.30.3.331

Dancygier AN, Karinski YS, Chacha A (2016) A model to assess the response of an arched roof of a lined tunnel. *Tunnelling and Underground Space Technology* 56(1):211-225, DOI: 10.1016/j.tust.2016.03.009

Horn M (1961) Horizontal earth pressure on perpendicular tunnel face. Proceedings of the Hungarian National Conference of the Foundation Engineer Industry, Budapest, Hungary

Idinger G, Aklik P, Wu W, Borja RI (2011) Centrifuge model test on the face stability of shallow tunnel. *Acta Geotechnica* 6(2):105-117, DOI: 10.1007/s11440-011-0139-2

Ji XB, Ni PP, Marco B, Zhao W, Mei GX (2018) Earth pressure on shield excavation face for pipe jacking considering arching effect. *Tunnelling and Underground Space Technology* 72(1):17-27, DOI: 10.1016/j.tust.2017.11.010

Kirsch A (2010) Experimental investigation of the face stability of shallow tunnels in sand. *Acta Geotechnica* 5(1):43-62, DOI: 10.1007/

s11440-010-0110-7

Leca E, Dormieux L (1990) Upper and lower bound solutions for the face stability of shallow circular tunnels in frictional material. *Géotechnique,*40(4):581-606, DOI: 10.1680/geot1990.40.4.581

Lee CJ, Wu BR, Chen HT, Chiang KH (2006) Tunneling stability and arching effects during tunneling in soft clayey soil. *Tunnelling and Underground Space Technology* 21(2):119-132, DOI: 10.1016/j.tust.2005.06.003

Li Y, Emeriault F, Kastner R, Zhang ZX (2009) Stability analysis of large slurry shield driven tunnel in soft clay. *Tunnelling and Underground Space Technology* 24(4):472-481, DOI: 10.1016/j.tust.2008.10.007

Liu W, Zhao Y, Shi P, Li J, Gan PL (2017) Face stability analysis of shield-driven tunnels shallowly buried in dry sand using 1-g large-scale model tests. *Acta Geotechnica* 13(1):1-13, DOI: 10.1007/s11440-017-0607-4

Lv XL, Zhou YC, Huang MS, Li FD (2017) Computation of the minimum limit support pressure for the shield tunnel face stability under seepage condition. *International Journal of Civil Engineering* 15(6):849-863, DOI: 10.1007/s40999-016-0116-0

Lv XL, Zhou YC, Huang MS, Zeng S (2018) Experimental study of the face stability of shield tunnel in sands under seepage condition. *Tunnelling and Underground Space Technology* 74:195-205, DOI: 10.1016/j.tust.2018.01.015

Min FL, Zhu W, Han XR (2013) Filter cake formation for slurry shield tunneling in highly permeable sand. *Tunnelling and Underground Space Technology* 38(3):423-430, DOI: 10.1016/j.tust.2013.07.024

Min FL, Zhu W, Lin C, Guo XJ (2015) Opening the excavation chamber of the large-diameter size slurry shield: A case study in Nanjing Yangtze River Tunnel in China. *Tunnelling and Underground Space Technology* 46:18-27, DOI: 10.1016/j.tust.2014.10.002

Ni PP, Moore ID, Take WA (2018) Distributed fibre optic sensing of strains on buried full-scale PVC pipelines crossing a normal fault. *Géotechnique* 68(1):1-17, DOI: 10.1680/jgeot.16.P.161

Soubra AH (2000) Three-dimensional face stability analysis of shallow circular tunnels. Proceedings of the international conference on geotechnical and geological engineering, November 19-24, Melbourne, Australia

Stanier SA, Blaber J, Take WA, White DJ (2015) Improved image-based deformation measurement for geotechnical applications. *Canadian Geotechnical Journal* 53(5):727-739, DOI: 10.1139/cgj-2015-0253

Subrin D, Wong H (2002) Tunnel face stability in frictional material: A new 3D failure mechanism. *Comptes Rendus Mecanique* 330:513-519 (in French)

Take WA (2015) Thirty-sixth canadian geotechnical colloquium: Advances in visualization of geotechnical processes through digital image correlation. *Canadian Geotechnical Journal* 52(9):1199-1220, DOI: 10.1139/cgj-2014-0080

Terzaghi K (1936) Stress distribution in dry and in saturated sand above a yielding trap-door. In: Proceedings of the international conference on soil mechanics, vol. 1. Harvard University Press, Cambridge, MA, USA, 307-311

Tognon AR, Rowe RK, Brachman RWI (1999) Evaluation of side wall friction for a buried pipe testing facility. *Geotextiles and Geomembranes* 17(4):193-212, DOI: 10.1016/s0266-1144(99)00004-7

Vermeer PA, Ruse NM, Marcher T (2002) Tunnel heading stability in drained ground. *Felsbau* 20(6):8-18

Wang MS (2008) Current developments and technical issues of underwater traffic tunnel-discussion on construction scheme of Taiwan strait undersea railway tunnel. *Chinese Journal of Rock Mechanics and Engineering* 27(11):2161-2172, DOI: 10.3321/j.issn:1000-6915.2008.11.001 (in Chinese)

White DJ, Take WA, Bolton MD (2003) Soil deformation measurement using particle image velocimetry (PIV) and photogrammetry. *Geotechnique* 53(7):619-631, DOI: 10.1680/geot.53.7.619.37383

Wu L, Guan T, Lei L (2013) Discrete element model for performance analysis of cutterhead excavation system of EPB machine. *Tunnelling and Underground Space Technology* 37(6):37-44, DOI: 10.1016/j.tust.2013.03.003

Yoo C, Shin H (2002) Deformation behaviour of tunnel face reinforced with longitudinal pipes – Laboratory and numerical investigation. *Tunnelling and Underground Space Technology* 18(4):303-319, DOI: 10.1016/S0886-7798(02)00101-3

Zhang ZX, Hu XY, Scott KD (2011) A discrete numerical approach for modeling face stability in slurry shield tunnelling in soft soils. *Computers and Geotechnics* 38(1):94-104, DOI: 10.1016/j.compgeo.2010.10.011

Zhang HF, Zhang P, Zhou W, Dong S, Ma BS (2016) A new model to predict soil pressure acting on deep burial jacked pipes. *Tunnelling and Underground Space Technology* 60:183-196, DOI: 10.1016/j.tust.2016.09.005